LiDAR DERIVED SALT MARSH TOPOGRAPHY AND BIOMASS: DEFINING ACCURACY AND SPATIAL PATTERNS OF UNCERTAINTY

T. Blount[1]*, S. Silvestri[2], M. Marani[3], A. D'Alpaos[1]

[1] Dept. of Geosciences, University of Padova, Padova, Italy – teganrose.blount@phd.unipd.it, andrea.dalpaos@unipd.it
[2] Dept. of Biological, Geological, and Environmental Sciences, University of Bologna, Ravenna, Italy - sonia.silvestri5@unibo.it
[3] Dept. of Civil, Environmental and Architectural Engineering, University of Padova, Padova, Italy - marco.marani@unipd.it

KEY WORDS: Remote Sensing, Light detection and ranging (LiDAR), Unmanned Aerial Vehicle (UAV), Digital elevation model (DEM), Tidal Wetlands, Biomass, Venice Lagoon, Blue Carbon.

ABSTRACT:

As valuable and vulnerable blue carbon ecosystems, salt marshes require adaptable and robust monitoring methods that span a range of spatiotemporal scales. The application of unmanned aerial vehicle (UAV) based remote sensing is a key tool in achieving this goal. Due to the particular characteristics of tidal wetlands, however, there are challenges in obtaining research and management relevant data with the requisite level of accuracy. In this study, the spatial patterns in uncertainty stemming from scan angle, binning method, vegetation structure and platform surface morphology are examined in the context of UAV light detection and ranging (LiDAR) derived digital elevation models (DEM). The results demonstrate that overlapping the UAV flight paths sufficiently to avoid sole reliance on LIDAR data with scan angles exceeding 15 degrees is advisable. Furthermore, the spatial arrangement of halophyte species and marsh morphology has a clear influence on DEM accuracy. The largest errors were associated with sudden structural transitions at the marsh channel boundaries. The DEM_{mean} was found to be the most accurate for bare ground, while the DEM_{min} was the most accurate for channels and the middle to high marsh vegetation (MAEs = -0.01m). For the low to middle vegetation, all the trialled DEMs returned a similar magnitude of mean error (MAE = -/+0.03m). The accuracy difference between the two vegetation associations examined appears to be connected to variations in coverage, height and biomass. Overall, these findings reinforce the link between salt marsh biogeomorphic complexity and the spatial distribution and magnitude of LiDAR DEM error.

1. INTRODUCTION

Tidal wetlands are an acknowledged source of many crucial ecosystem services (Barbier et al., 2011; D'Alpaos and D'Alpaos, 2021). For instance, as a blue carbon ecosystem (BCE), they have an accentuated ability to produce, trap and ultimately form influential long-term reservoirs of organic carbon (Duarte et al., 2005; McLeod et al., 2011; Trettin and Jurgensen, 2003). Globally the integrity and size of salt marsh ecosystems have been much depleted and remain under threat from human and environmental generated pressures (Rogers and Woodroffe, 2015; Valiela et al., 2009). Since the loss of salt marshes reduces carbon reservoirs and releases existing stocks as greenhouse gases (Pendleton et al., 2012), salt marsh sustainable restoration and conservation is of high priority in climate mitigation and adaptation (Lovelock and Duarte, 2019). There is a need for the development of methods and frameworks that are able to efficiently monitor key salt marsh parameters of interest. Furthermore, it is necessary to improve the understanding of intricate salt marsh processes and responses that remain, as yet, ill defined.

Salt marshes are difficult to characterise in a detailed spatially explicit manner using field sampling techniques alone. This is due to the expansive isolated areas which these ecosystems occupy; the platform's low topographic and vegetative reliefs; the difficulties inherent to traversing quagmires and; the high ecogeomorphic complexity of this landscape, rife with inseparable biotic and abiotic processes. Given these challenges, remote sensing is a key aspect of the integrated multidisciplinary approach required to effectively and affordably study salt marshes across a range of spatiotemporal scales.

The derivation of accurate digital elevation and vegetation models are of particular importance to salt marsh research as they can support many applications such as ecosystem scale modelling and carbon sequestration assessments. Unmanned aerial vehicle (UAV) based remote sensing techniques are well suited to the salt marsh context and thus far UAV light detection and ranging (LiDAR) has proven adept for deriving such models (e.g., Curcio et al., 2022; Hladik and Alber, 2012; Pinton et al., 2021). There are however still substantial uncertainties associated with salt marsh terrain and vegetation models whose origins remain insufficiently defined. This research aimed to (1) qualitatively and quantitatively elucidate the accuracy associated with UAV LiDAR derived salt marsh elevation models and; (2) examine the origins of any spatial patterns of uncertainty encountered. The second part of the analysis focused on the effect which specific LiDAR acquisition parameters, product generation methodology, vegetation characteristics and geomorphology have on the accuracy.

2. MAIN BODY

2.1 Study Area

The study site covers approximately 0.47 km^2 of the San Felice salt marshes, which are situated in the north eastern section of the Venice Lagoon, Italy (Figure 1). The lagoon has an area of 550

* Corresponding author

km^2, an average depth of 1.0-1.5 m, a semidiurnal microtidal regime and a tidal range of around 1 m (D'Alpaos et al., 2013; Ghinassi et al., 2018). The lagoon is a barrier island system with three inlets connecting to the northern Adriatic Sea. Extensive and long-term human occupation has altered the lagoon system regime, resulting in a negative sediment budget and significant geomorphologic and hydraulic changes (Carniello et al., 2009). These anthropogenic effects are also coupled with environmental pressures intensified by climate change. The extent of the lagoon's salt marsh areas has reduced over the last two centuries by 137 km^2, a 76% decrease which leaves a remaining area of about 43 km^2 (Carniello et al., 2009; D'Alpaos, 2010). The salt marsh area loss rate is not uniform across the lagoon. The San Felice salt marshes are located in the northern zone, which has relatively less intense lateral erosion rates recorded in comparison to the central and southern sections of the lagoon (Bendoni et al., 2016; Day et al., 1998; Tommasini et al., 2019).

Figure 1. San Felice study area extent (Venice Lagoon, Italy) with the GNSS ground control point (GCP) distribution.

The halophytic species most notably present on the San Felice salt marshes are: *Limonium narbonense, Sarcocornia fruticose, Juncus maritimus, Salicornia veneta, Pucinellia palustris, Inula crithmoides, Spartina maritima,* and of late, *Spartina anglica*. It has been well established that these halophyte species form vegetation associations which are closely linked to elevation and as such local geomorphologic characteristics (Belluco et al., 2006; Marani et al., 2006; Silvestri et al., 2003; Wang et al., 2007; Yang et al., 2020).

2.2 Materials

The datasets used in this study were acquired on 5 to 11 of September 2021. The UAV flights were undertaken alongside *in situ* measurements of above ground biomass (53 in total) and topographic GNSS points. These samples were distributed across the study area and cover a range of biogeomorphological associations. In total, 591 topographic points were collected using a Real-Time Kinematic Differential Global Positioning System (Leica Viva GNSS GS15 RTK GPS). Out of these, 28 were ground control points (GCP) taken at the centre of 0.5 metre square targets (locations shown in Figure 1C). An orthophoto was also derived from the dataset acquired by the deployed UAV. The orthophoto was generated using the Agisoft Metashape software and it has a spatial resolution of 2.5 cm and three spectral bands (RGB). The UAV survey and *in situ* datasets have geodetic vertical units in metres relative to mean sea level (m.s.l.) and the coordinate system used was WGS84 UTM Zone 33N. The LiDAR UAV flight and point cloud details are summarised in Table 1 below. The LiDAR point cloud used in this analysis was pre-processed using the following software: DJI Terra-Pro (alignment and scan optimisation), Terrascan (overlap elimination) and Terra Match (georeferencing).

LiDAR Survey	
UAV model	DJI Matrice 300 RTK
Sensor	L1 & 20 MP RGB
Scan angle range	35 to -35 degrees
Scan mode	Non-repetitive
Frequency	180 Hz
Number of echoes	3
Lateral overlap	30%
Flight velocity	5 m/s
Flight altitude	100 m
Area covered	473,676 m^2
Number of points	82.6 million
Average point density	174.3 points/m^2
Average distance between points	0.07 m

Table 1. UAV survey and processed dataset details.

2.3 Method

2.3.1 LiDAR cloud processing and DEM derivation

During the analysis the LiDAR point cloud was processed and manipulated directly using RStudio (R Core Team, 2022). Prior to creating the DEMs, the point cloud was filtered for duplicate points, extreme angles (>=26 degrees) and outliers ('noise'). The outlier removal method applied was the Median and Interquartile Deviation Method (IQD). Prior to selecting this method, testing was carried out to confirm that DEM accuracy improved after removing the 'noise' using IQD. The DEM grid resolution chosen for the analysis was 0.25 m, since this was found to be the resolution at which there was a balance between the need for accuracy from both a spatial resolution and a point density perspective. Three types of DEMs were generated by calculating: (1) 'grid min' which is the minimum LiDAR point elevation present within each grid cell; (2) 'grid mean' which is the mean of the LiDAR elevations present in each grid cell and; (3) 'nearest point' which is the elevation of the LiDAR point nearest to the GNSS point located within the grid. ArcGIS (ESRI Inc., 2023) and MATLAB (The MathWorks Inc., 2022) were used to visualise, query and cross-check the GNSS points and the orthophoto with the output from RStudio.

2.3.2 Scan angle and biogeomorphic associations

For each of the 591 GNSS points, key parameters of potential influence were assigned in order to allow the exploration of their effect on the spatial accuracy of the three DEMs. Firstly, the scan angle was defined as the mean scan angle for the mean DEM and the specific point scan angle for the minimum and nearest point DEMs. Next, points were assigned geomorphic classes according to whether they were GCPs or otherwise being located in channels, on bare ground or on vegetated salt marsh surfaces. The points from the vegetated salt marsh surfaces were then divided anew into broad dominant halophytic species associations as described in Table 2 below. The associations were ascertained based on *in situ* biomass samples and expert visual assessment of the high resolution orthophotograph.

Dominant species association	Vegetation class
Inula cri. *Juncus mar.* *Sarcocornia fru.*	*High/Mid Marsh*
Limonium nar. *Spartina mar.* *Spartina ang.*	*Mid/Low Marsh*

Salicornia ven.	

Table 2. Halophytic species associations and overarching classes.

The data was then analysed to derived the errors associated with each of these specific vegetation associations and they were regrouped into two overarching classes in accordance with their location on the marsh gradient, their biomass and their effect on the accuracy of the DEM. The first overarching class was 'High/Mid Marsh' which consists of associations dominated by *Inula cri.*, *Juncus mar.* and *Sarcocornia fru.* The second class was 'Mid/Low marsh' which includes *Limonium nar.*, *Spartina mar.*, *Spartina ang.* and *Salicornia ven.* dominated associations. The number of GNSS points assigned to each class were 254 and 257 respectively.

2.3.3 Accuracy analysis

To analyse the LiDAR elevation error associated with the different classes and DEMs, two measures were applied. The mean absolute error (MAE) and the root mean square error (RMSE) were calculated as per Equations (1) and (2) below respectively.

$$MAE = \frac{\sum_{i=1}^{N}(z_0 - z_1)}{n}; \quad (1)$$

$$RMSE = \sqrt{\frac{\sum_{i=1}^{N}(z_0 - z_1)^2}{n}}; \quad (2)$$

where i = ith sampling point
z_0 = the GNSS elevation
z_1 = the LiDAR elevation
n = the number of points in the dataset

These values were calculated for the mean, minimum and nearest point LiDAR DEMs for all biogeomorphic classes and the GCPs. Linear regression analysis was also performed to assess the fit of the LiDAR data to the GNSS data for the aforementioned combinations.

2.4 Results

For all the DEMs and classes analysed, including the GCPs, there was a constant trend that the DEM error behaviour was not consistent as the scan angle increased. Instead, once the scan angle began to increase above 10 degrees, a gradual downwards drift in the errors manifests. Furthermore, the spread and magnitude of the errors increases notably after 15 degrees was surpassed. This heterogenous error behaviour with increasing scan angle can be exemplified by Figure 2 which shows the results for the mean DEM. It was also found that in the LiDAR point cloud the scan angle is inversely correlated to point density. Between 10 and 25 degrees the point density drops on average in a linear manner from 75 to 50 points/m^2.

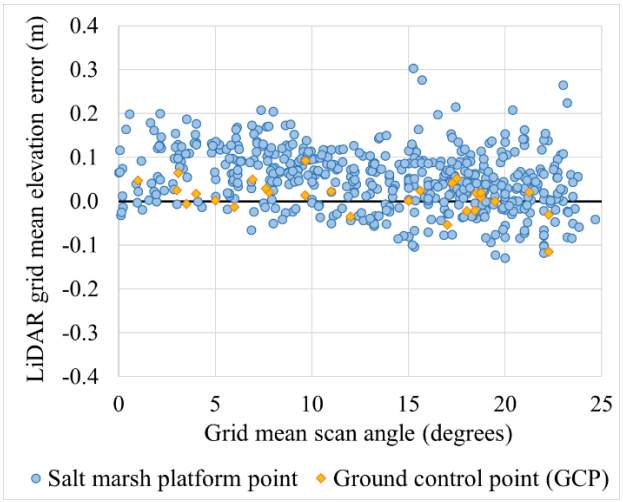

Figure 2. Plot showing the relationship between mean scan angle and the LiDAR mean DEM elevation error for all GNSS salt marsh platform points and the ground control points (GCPs).

The linear regression results for the 28 GCPs are shown in Figure 3. It is evident that the nearest point DEM has a similar performance to the mean grid DEM and that the minimum grid DEM leads to under estimation of the GCP surface and more outliers. The linear regression performed for the bare marsh surfaces showed a similar trend but with a slightly reduced level of correlation. The linear regression results for the vegetation species associations ranged from poor to fair, the High/Mid Marsh associations were amongst the latter. The linear regression for the channel points had practically zero signs of correlation on all of the DEMS.

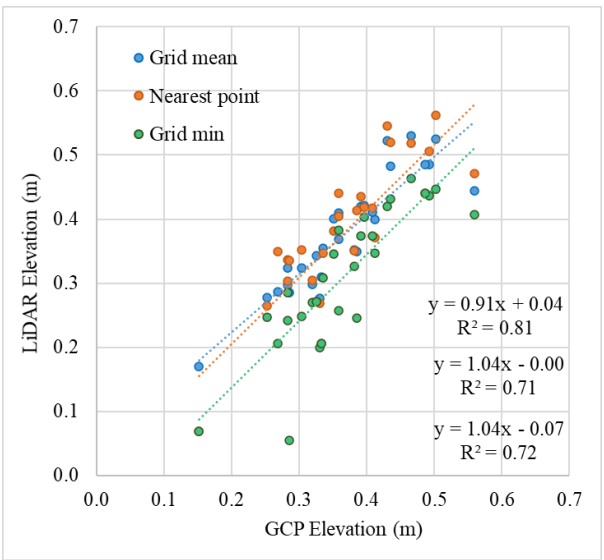

Figure 3. Linear regression of LiDAR elevation and GNSS GCP elevation for the minimum grid, mean grid and nearest point LiDAR DEMs.

The evaluation of DEM error, using the MAE and RMSE measurements, found that when the marsh platform is assessed as a whole, the DEMs' RMSEs were of a similar magnitude of around 8 to 9 cm. But the mean absolute errors were more diverse. As a negative MAE represents an elevation overestimate, the overall marsh MAE_{min} translates as a 1 cm underestimate and

the associated MAE_{mean} and $MAE_{nearest}$ as 5 cm overestimates. When the whole marsh is broken into its overarching biogeomorphic classes, however, a more diverse picture appears as can be seen in Figure 4.

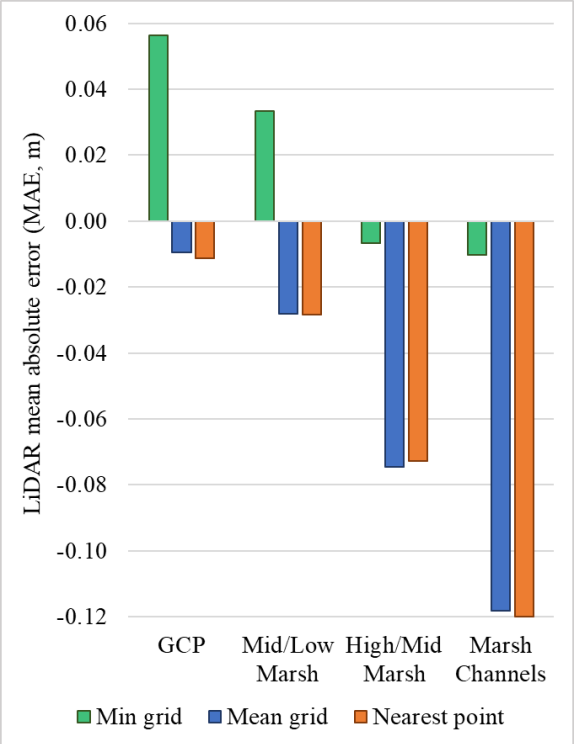

Figure 4. The LiDAR mean absolute error (MAE) evaluated for the minimum, mean and nearest point DEMs for the following classes (1) ground control points (GCP); (2) middle to low marsh zone; (3) middle to high marsh zone and; (4) channels within the marsh.

It is clear from this plot that the MAE_{min} results give underestimates of the elevation for the GCPs (5.6 cm) and the Mid/Low Marsh (3.3 cm), however, it is by far the best estimate of the High/Mid Marsh and the channels. MAE_{min} for the latter cases has only a small mean elevation overestimate in the order of 0.7-1.0 cm compared to the other DEMs which give an elevation overestimate in the 7.0-12.0 cm range. The DEM_{min} also gives a significantly lower RMSE for the channel and High/Mid Marsh classes (8.0-10.0 cm) compared to the nearest point and grid mean DEMs (10.0-18.0 cm).

The DEM_{mean} still overestimates but becomes the most accurate estimate in the case of the GCP and Mid/Low Marsh classes. In these cases the MAE_{mean} is an overestimate of 1.0 cm and 2.8 cm and the $RMSE_{mean}$ is 4.0 cm and 6.0 cm respectively. Although for the GCP it is clear that the DEM_{mean} is the most accurate by far, for the Mid/Low Marsh the results for DEM_{min} and $DEM_{nearest}$ are not so markedly worse. For this class, all the DEMs will give a MAE error in the order of 3.0 cm and a RMSE in the order of 7.0 cm. The main difference between them is that the DEM_{min} is an elevation underestimate.

The average dry biomass, vegetation height and marsh elevation for the two vegetation classes was investigated. It was seen that the High/Mid Marsh is characterised by almost three times the average dry biomass density and twice the vegetation height of the Mid/Low Marsh category. The surface elevation of the latter class is also on average 10 cm lower.

2.5 Discussion

The scan angle drift in the elevation error present across all the DEMs introduces an extra layer of inconsistency into the dataset. Given the direct inverse relationship between scan angle and point density in this dataset, the point density is also potentially having an effect on the level of accuracy. Thus, flight paths with significant overlaps in the order of 70% that reduce the reliance on points with larger scan angles and lower densities are recommended as a mitigation technique.

The GCP points are bare of surface vegetation and for these the mean and the nearest DEMs provide better estimates than the minimum grid. Similarly, Curcio et al. (2022) found that due to the high level of scattering caused by salt marsh bare ground, taking the mean in these bare areas gave the higher accuracy as well. The influence of this ground scattering trend can also be seen in the behaviour of the Mid/Low Marsh class, which consists of shorter and more sparse vegetation associations. In this class it is less likely that the minimum point is the only point to reach the ground, as is often the case for the taller and denser high and middle marsh vegetation where the DEM_{min} is more accurate (e.g., Pinton et al., 2021).

The elevations of the channels etched in the marsh are without doubt best represented by the DEM_{min} and this morphology's high variation in error is likely due to the abrupt change in morphological structure that takes place on the transition between salt marsh platform and channel. This has been noted in other studies, in some cases resulting in an underestimation error instead (e.g., Pinton et al., 2020). Furthermore, another factor that may be influencing the accuracy in the low inner marsh (included in the Mid/Low Marsh class) and the channels, is the more predominant presence of wet soil surfaces which can also adversely affect the LiDAR DEM accuracy (e.g., Schmid, 2011).

The results established that when the points are separated into classes, the errors exhibited can significantly vary from the overall average due to spatial variability in uncertainty. Hence, the biogeomorphic characteristics of the environment need to be accounted for when considering the necessary level of accuracy and the choice of DEM derivation method most suited for the area of interest. In addition, this analysis contributes to the on-going need for accuracy studies focusing on a range of salt marsh environments and species assemblages in order to fully elucidate the drivers of salt marsh DEM inaccuracy. Accurate DEMs are important for many relevant applications, such as deriving above ground biomass maps. Furthermore, they are also crucial for modelling and predicting ecosystem responses to external pressures such as sea-level rise and anthropogenic activities.

3. CONCLUSIONS

This study endeavoured to qualitatively and quantitatively examine the spatial accuracy associated with UAV LiDAR derived salt marsh digital elevation models based on minimum, mean and nearest point binning. The spatial patterns of uncertainty encountered demonstrated linkages to the variables examined. Firstly, increasing scan angle and decreasing point density, results in a gradual but notable downwards elevation

error drift and an increase in error extremes once an angle of about 15 degrees is exceeded.

Secondly, the accuracy is affected by the halophyte species association and overarching vegetation class which is in turn intrinsically linked to the geomorphologic structures present in the marsh. It was found that channels retained the highest overestimation inaccuracies which are likely due to sudden changes in elevation. The presence of water in channels and the inner marsh, however, may also be reducing the level of accuracy.

Thirdly, it was found that DEM grids based on binning the minimum value are more accurate for middle to high marsh zones and channels while mean binning based DEM grids are more accurate for the middle to low marsh zone and bare surfaces. As the DEM accuracy is highly sensitive to the presence and structure of above ground biomass this aspect is particularly relevant in defining the uncertainties of salt marsh above ground biomass and hence carbon sequestration capacity maps derived from LiDAR.

ACKNOWLEDGEMENTS

The authors would like to acknowledge the contributions of Archetipo s.r.l, Marco Assiri, Ruth Cuenca, Olinda Rufo, Guillaume Goodwin and the European Commission under the Erasmus Mundus Joint Master Degree Programme in Water and Coastal Management [grant number 586596-EPP-1-2017-1-IT-EPPKA1-JMD-MOB]. This material is based upon work supported by the National Science Foundation under Grant No. 2016068, project title: "Coupled Ecological-Geomorphological Response of Coastal Wetlands to Environmental Change".

REFERENCES

Barbier, E.B., Hacker, S.D., Kennedy, C., Koch, E.W., Stier, A.C., Silliman, B.R., 2011: The value of estuarine and coastal ecosystem services. *Ecol. Monogr.*, 81, 169–193. doi.org/10.1890/10-1510.1.

Belluco, E., Camuffo, M., Ferrari, S., Modenese, L., Silvestri, S., Marani, A., Marani, M., 2006: Mapping salt-marsh vegetation by multispectral and hyperspectral remote sensing. *Remote Sens. Environ.*, 105, 54–67. doi.org/10.1016/j.rse.2006.06.006.

Bendoni, M., Mel, R., Solari, L., Lanzoni, S., Francalanci, S., Oumeraci, H., 2016: Insights into lateral marsh retreat mechanism through localized field measurements. *Water Resour. Res.*, 52, 1446–1464. doi.org/10.1002/2015WR017966.

Carniello, L., Defina, A., D'Alpaos, L., 2009: Morphological evolution of the Venice lagoon: Evidence from the past and trend for the future. *J. Geophys. Res. Earth Surf.*, 114, 1–10. doi.org/10.1029/2008JF001157.

Curcio, A.C., Peralta, G., Aranda, M., Barbero, L., 2022: Evaluating the Performance of High Spatial Resolution UAV-Photogrammetry and UAV-LiDAR for Salt Marshes: The Cádiz Bay Study Case. *Remote. Sens.*, 14, 3582. doi.org/10.3390/rs14153582.

D'Alpaos, A., Carniello, L., Rinaldo, A., 2013: Statistical mechanics of wind wave-induced erosion in shallow tidal basins: Inferences from the Venice Lagoon. *Geophys. Res. Lett.*, 40, 3402–3407. doi.org/10.1002/grl.50666.

D'Alpaos, C., D'Alpaos, A., 2021: The Valuation of Ecosystem Services in the Venice Lagoon: A Multicriteria Approach. *Sustainability*, 13, 9485. doi.org/10.3390/su13179485.

D'Alpaos L. 2010: *Fatti e misfatti di idraulica lagunare. La laguna di Venezia dalla diversione dei fiumi alle nuove opere delle bocche diporto*. Istituto Veneto di Scienze, Lettere e Arti, Venice.

Day, J.W., Scarton, F., Rismondo, A., Are, D., 1998: Rapid Deterioration of a Salt Marsh in Venice Lagoon, Italy. *J. Coast. Res.*, 14, 583–590.

Duarte, C.M., Middelburg, J.J., Caraco, N., 2005: Major role of marine vegetation on the oceanic carbon cycle. *Biogeosciences*, 1, 1–8.

ESRI Inc., 2023. ArcGIS Desktop (ArcGIS) Software, Version 10.8.2. ESRI Inc. www.esri.com (2 March 2023).

Ghinassi, M., D'alpaos, A., Gasparotto, A., Carniello, L., Brivio, L., Finotello, A., Roner, M., Franceschinis, E., Realdon, N., Howes, N., Cantelli, A., 2018: Morphodynamic evolution and stratal architecture of translating tidal point bars: Inferences from the northern Venice Lagoon (Italy). *Sedimentology*, 65, 1354–1377. doi.org/10.1111/sed.12425.

Hladik, C., Alber, M., 2012: Accuracy assessment and correction of a LIDAR-derived salt marsh digital elevation model. *Remote Sens. Environ.*, 121, 224–235. doi.org/10.1016/j.rse.2012.01.018.

Lovelock, C.E., Duarte, C.M., 2019: Dimensions of Blue Carbon and emerging perspectives. *Biol. Lett.*, 15, 20180781. doi.org/10.1098/rsbl.2018.0781.

Marani, M., Belluco, E., Ferrari, S., Silvestri, S., D'Alpaos, A., Lanzoni, S., Feola, A., Rinaldo, A., 2006: Analysis, synthesis and modelling of high-resolution observations of salt-marsh eco-geomorphological patterns in the Venice lagoon. *Estuar. Coast. Shelf Sci.*, 69, 414–426. doi.org/10.1016/j.ecss.2006.05.021.

McLeod, E., Chmura, G.L., Bouillon, S., Salm, R., Björk, M., Duarte, C.M., Lovelock, C.E., Schlesinger, W.H., Silliman, B.R., 2011: A blueprint for blue carbon: toward an improved understanding of the role of vegetated coastal habitats in sequestering CO2. *Front. Ecol. Environ.*, 9, 552–560. doi.org/10.1890/110004.

Pendleton, L., Donato, D.C., Murray, B.C., Crooks, S., Jenkins, W.A., Sifleet, S., Craft, C., Fourqurean, J.W., Kauffman, J.B., Marbà, N., Megonigal, P., Pidgeon, E., Herr, D., Gordon, D., Baldera, A., 2012: Estimating Global "Blue Carbon" Emissions from Conversion and Degradation of Vegetated Coastal Ecosystems. *PLoS. One.*, 7, e43542. doi.org/10.1371/journal.pone.0043542.

Pinton, D., Canestrelli, A., Wilkinson, B., Ifju, P., Ortega, A., 2021: Estimating Ground Elevation and Vegetation Characteristics in Coastal Salt Marshes Using UAV-Based LiDAR and Digital Aerial Photogrammetry. *Remote Sens.*, 13, 4506. doi.org/10.3390/rs13224506.

Pinton, D., Canestrelli, A., Wilkinson, B., Ifju, P., Ortega, A., 2020: A new algorithm for estimating ground elevation and vegetation characteristics in coastal salt marshes from high-resolution UAV-based LiDAR point clouds. *Earth Surf. Process. Landf.*, 45, 3687–3701. doi.org/10.1002/esp.4992.

R Core Team, 2022. R: A Language and Environment for Statistical Computing Software, Version 4.2.1 (2022-06-23 ucrt)

-- "Funny-Looking Kid". The R Foundation for Statistical Computing. R-project.org (29 7 2022).

Rogers, K., Woodroffe, C.D., 2015: Tidal Flats and Salt Marshes, in: Masselink, G., Gehrels, R. (Eds.), *Coastal Environments and Global Change*. John Wiley & Sons, Ltd, Chichester, UK, pp. 227–250. doi.org/10.1002/9781119117261.

Schmid, K., Hadley, B., Wijekoon, N., 2011: Vertical Accuracy and Use of Topographic LIDAR Data in Coastal Marshes. *Journal of Coastal Research*, 27, 116-132. doi.org/10.2307/41315921.

Silvestri, S., Marani, M., Marani, A., 2003: Hyperspectral remote sensing of salt marsh vegetation, morphology and soil topography. *Physics and Chemistry of the Earth*, Parts A/B/C 28, 15–25. doi.org/10.1016/S1474-7065(03)00004-4.

Tommasini, L., Carniello, L., Ghinassi, M., Roner, M., D'Alpaos, A., 2019: Changes in the wind-wave field and related salt-marsh lateral erosion: inferences from the evolution of the Venice Lagoon in the last four centuries. *Earth Surf. Process. Landf.*, 44, 1633–1646. doi.org/10.1002/esp.4599.

The MathWorks Inc., 2022. MATLAB Software, Version 9.13.0 (R2022b). The MathWorks Inc. www.mathworks.com (14 Dec 2022).

Trettin, C.C., Jurgensen, M.F., 2003: Carbon Cycling in Wetland Forest Soils, in: Kimble, J.M., Heath, L.S., Birdsey, R.A., Lal, R. (Eds.), *The Potential of U.S. Forest Soils to Sequester Carbon and Mitigate the Greenhouse Effect*. CRC Press, Boca Raton, pp. 311–331.

Valiela, I., Kinney, E., Culbertson, J., Peacock, E., Smith, S., 2009: Global Losses of Mangroves and Salt Marshes, in: Duarte, C.M. (Ed.), *Global Loss of Coastal Habitats Rates, Causes and Consequences*. Fundación BBVA, p. 142.

Wang, C., Menenti, M., Stoll, M.P., Belluco, E., Marani, M., 2007: Mapping mixed vegetation communities in salt marshes using airborne spectral data. *Remote Sens. Environ*., 107, 559–570. doi.org/10.1016/j.rse.2006.10.007.

Yang, Z., D'Alpaos, A., Marani, M., Silvestri, S., 2020: Assessing the fractional abundance of highly mixed salt-marsh vegetation using random forest soft classification. *Remote Sens*., 12, 1–25. doi.org/10.3390/rs12193224.

APPENDIX A: SOFTWARE PACKAGES

Bivand, R., Rundel, C., 2021: _rgeos: Interface to Geometry Engine - Open Source ('GEOS')_. R package version 0.5-9, CRAN.R-project.org/package=rgeos.

Bivand R., Keitt T, Rowlingson B., 2022: _rgdal: Bindings for the 'Geospatial' Data Abstraction Library_. R package version 1.5-32, CRAN.R-project.org/package=rgdal.

Gräler, B., Pebesma, E., Heuvelink, G., 2016: Spatio-Temporal Hijmans, R., 2022: _raster: Geographic Data Analysis and Modeling_. R package version 3.5-21, CRAN.R-project.org/package=raster.

Interpolation using gstat. *The R Journal*, 8(1), 204-218.

Isenburg, M., 2023: LAStools - efficient LiDAR processing software, Version 141017 academic, rapidlasso.com/LAStools (27 Feb 2023).

Kuhn, M., 2022: _caret: Classification and Regression Training_. R package version 6.0-92, CRAN.R-project.org/package=caret.

Pebesma, E., 2004: Multivariable geostatistics in S: the gstat package. *Computers & Geosciences*, 30, 683-691.

Roussel J., Qi J., 2020: _RCSF: Airborne LiDAR Filtering Method Based on Cloth Simulation_. R package version 1.0.2, CRAN.R-project.org/package=RCSF.

Roussel, J., Auty, D., Coops, N., Tompalski, P., Goodbody, T., Sánchez Meador, A., Bourdon, J., De Boissieu, F., Achim, A., 2020: lidR : An R package for analysis of Airborne Laser Scanning (ALS) data. *Remote Sensing of Environment*, 251 (August), 112061. doi:10.1016/j.rse.2020.112061.

Roussel, J.R., Auty, D., 2022: Airborne LiDAR Data Manipulation and Visualization for Forestry Applications. R package version 4.0.1. cran.r-project.org/package=lidR.

Urbanek, S., Johnson, K., 2022: _tiff: Read and Write TIFF Images_. R package version 0.1-11, https://CRAN.R-project.org/package=tiff.

Wickham, H., 2016: ggplot2: Elegant Graphics for Data Analysis. Springer-Verlag New York.

Wickham, H., Bryan, J., 2022: _readxl: Read Excel Files_. R package version 1.4.0, CRAN.R-project.org/package=readxl.

Wickham, H., François, R., Henry, L., Müller, K., 2022: _dplyr: A Grammar of Data Manipulation_. R package version 1.0.9, CRAN.R-project.org/package=dplyr.